Birkhoff normal forms and stability indicators for betatronic motion

G. Turchetti *

*Department of Physics and Astronomy, Alma Mater Studiorum – University of Bologna, Via Irnerio 46, 40-126 Bologna, Italy
E-mail: giorgio.turchetti@unibo.it

F. Panichi **

**Institute of Physics and CASA*, Faculty of Mathematics and Physics, University of Szczecin, Wielkopolska 15, 70-451 Szczecin, Poland
E-mail: federico.panichi@stud.usz.edu.pl

Celestial and beam dynamics are similar and share the same methods for the stability analysis. The perturbation theory is the main analytical tool and its version for the symplectic maps, which describe the transverse motion in circular accelerators, are the Birkhoff normal forms. They allow to evaluate the dynamic aperture when the frequency is close to an unstable resonance and to estimate the stability time when it is far from low order resonances. In celestial mechanics the numerical analysis of stability is usually based on the Lyapunov error (for instance, the Fast Lyapunov Indicator). In the case of symplectic maps the forward and reversibility errors induced by random perturbations have been proposed. The use of non-resonant normal forms allows to establish the power law asymptotic behavior of errors with the corresponding pre-factors. The error plots in a phase plane, obtained by fixing the missing coordinates, allow to establish the stability properties of each orbit. The reversibility error due to round-off jointly with the Lyapunov error provide an adequate stability pattern for the Hénon map and their use is suggested for more realistic models such as the one turn map in a ring.

Keywords: Celestial Mechanics ; Beam Dynamics ; Normal Forms ; Stability Analysis .

1. Introduction

Celestial mechanics and beam dynamics are based on the Hamiltonian formulation of the equations of motion of planets or protons in a circular ring. The stability of orbits after a large number of periods is the most relevant problem. In the two-body gravitational problem the circular orbit of a planet is stable, whereas the circular orbit of a charged particle moving in a uniform magnetic field is not. Indeed, in the last case a small component of the velocity along the magnetic field causes a drift along it. Some analogies exist between the planar restricted three-body problem[1] and the transverse motion of a flat beam in a non-linear lattice. A closer correspondence is found with the Hénon-Heiles[2] model describing the motion of a star in an elliptical galaxy. In this case there is a neighborhood $\mathcal{A}$ of the origin, preserved by the beam map or the Hénon-Heiles Poincaré map, out of which the orbits escape exponentially fast to infinity. The generic one turn map in a ring is 4D just as the Poincaré map of the non planar restricted three-body system. The

absence of topological barriers allows Arnold diffusion. As a consequence, finite time stability must be considered according to the Nekhoroshev theorem[3,4]. The stability times of interest in a planetary system or in a large hadron accelerator are comparable, typically billions of periods.

In order to investigate the geometry of orbits, perturbation methods were developed in celestial mechanics. For the Poincaré map the perturbative analysis near a linearly stable fixed point was developed by Birkhoff and was proposed as the natural tool to analyze the one turn map of a circular accelerator[5–7] and[8] with references therein. The method consists in finding a change of coordinates which transforms the given map into a new map invariant with respect to a continuous or discrete symmetry group.

The nature of an orbit with initial point $\mathbf{x}_0$ is investigated by looking at the displacement of an initial condition, starting at $\mathbf{x}_0 + \epsilon\boldsymbol{\eta}_0$ with $\|\boldsymbol{\eta}\| = 1$. After n iterations the displacement is $\epsilon\,\boldsymbol{\eta}_n$ at first order in ϵ and the Lyapunov error can be defined as the norm of the normalized displacement $\|\boldsymbol{\eta}_n\|$. Its logarithm was first proposed as a fast indicator named Fast Lyapunov Indicator (FLI)[9]. Recently, the displacement $\epsilon\boldsymbol{\Xi}_n$ induced by small random perturbations was considered and the so called forward error (FE) was defined as the root mean square (rms) deviation of $\boldsymbol{\Xi}_n$. The reversibility error (RE) was defined as the rms of the normalized displacement $\boldsymbol{\Xi}_n^R$ from the initial point, and calculated after iterating the map forward and backward n times with an additive noise[10]. The growth of errors follows a power law for regular orbits, and an exponential law for chaotic orbits. For an integrable map the power law growth can be proved by using normal coordinates[11] and the result is extended here to quasi-integrable maps by using the normal forms theory.

In order to evaluate the LE, FE and RE for a given initial condition one needs to compute the orbit and the tangent map along it. If the tangent map is not available, LE can be evaluated by computing a second orbit for a close initial condition. This method to calculate the LE is known as the shadow-particle method, see[12] and references therein. The reversibility error can also be obtained as a consequence of the accumulation of round-off errors. The computation is based on the iteration of the map n times forward and backward. To summarize we propose two definitions of the reversibility error. The first one is defined as Reversibility Error (RE), where the perturbation introduced at each step is an additive noise with known statistical properties. The second one is the Reversibility Error Method (REM) where the perturbation at each step is the round-off error introduced by the numerical computations. The first definition is suitable for analytical estimates, the second one is trivial to implement and has a lower computational cost. The effectiveness of REM was first shown for the standard map[13] and appears to be be comparable with RE, for maps of sufficient computational complexity. In celestial mechanics, the Mean Exponential Growth of Near Orbits (MEGNO)[14,15] is commonly used. This is a filter introduced to kill the large oscillations often observed in the Lyapunov-based error methods (LE). For instance, MEGNO was successfully used to analyze the

stability of the few-body problem modelling planetary systems [16], the stability of asteroids [17,18] and satellites [19]. The REM procedure was successfully applied together with LE to analyze the orbital stability of exoplanets [11], a subject of growing interest in astronomy.
Establishing which is the best fast indicator is an open problem [11,13,20] and not always a single fast indicator is sufficient to correctly describe the phase space of a system. In this paper, we compare the analytical estimates with the numerical computation of the errors (LE, FE, RE, REM) for the 2D Hénon map and the agreement is excellent up to the dynamic aperture. The procedure described in this paper to investigate and characterize the dynamical structure of multi-dimensional Hamiltonian systems with or without integrals of motions is applied to a 4D map, modeling the transverse dynamics of a circular accelerator. We choose a 2D phase plane and fix the value of the remaining coordinates to compute the errors, which are visualized using a chromatic scale. If an Hamiltonian H interpolating the orbits is known, one can fix only the third coordinate and impose that the value of H is the same for all the initial conditions to determine the fourth coordinate. Though in this case the correspondence between the errors and the orbits of the Poincaré map for H can be analytically established, the complexity and numerical cost of the procedure (computation of an interpolating Hamiltonian using the normal forms and integration of its orbits via an implicit symplectic integrator) discourage its use. The LE and REM methods are immediate to implement when we fix the extra coordinates and do not require very long orbits. No more than one thousand iterations are enough to distinguish regular and chaotic orbits within the dynamic aperture Magnifications require a correspondingly higher number of iterations to detect finer details.
Since the REM procedure is extremely simple and numerically efficient, it can be applied to the one turn map of a realistic lattice. The number of iterations needed to reconstruct the phase space structure are low unless we are interested in the long term stability and dynamic aperture, but also in this case the computational challenge is affordable. The successful application to the orbital stability of exoplanets should encourage its use for circular accelerators.

2. Celestial mechanics models

In celestial mechanics the two simplest models showing a rich dynamical structure are the restricted planar three-body problem [1] and the Hénon-Heiles Hamiltonian [2]. The first one describes the motion of an asteroid subject to the attraction of a star of mass m_1 and a planet of mass $m_2 << m_1$, moving on circular orbits around their center of mass. The asteroid is assumed to move in the same plane as the massive bodies and to have a vanishingly small mass m_3 so that the motion of the star and the planet are not perturbed. Space coordinates and time are scaled so that the distance and the periods of the planet are equal to 1 (see for instance [21]). Denoting by x, y the space coordinates of the asteroid its Hamiltonian in the co-rotating

system is given by

$$H = \frac{1}{2}(p_x^2 + p_y^2) + yp_x - xp_y + V(x, y), \tag{1}$$

where V is the gravitational potential

$$V = -\frac{1-\mu}{(x+\mu)^2 + y^2} - \frac{\mu}{(x-1+\mu)^2 + y^2} \qquad \mu = \frac{m_2}{m_1 + m_2}. \tag{2}$$

For the sun-Jupiter system the mass ratio is $\mu = 0.000954$. The second term in the Hamiltonian, due to the rotation, implies that $p_x = \dot{x} - y,\ p_y = \dot{y} + x$. The Hamiltonian is an invariant of motion and can be written as

$$H = \frac{1}{2}(\dot{x}^2 + \dot{y}^2) + V_{\text{eff}} \qquad V_{\text{eff}} = -\frac{1}{2}(x^2 + y^2) + V, \tag{3}$$

where V_{eff} is the effective potential. Letting $H = E$ be the energy of the system the Jacobi invariant is $J = -2E$. There are 5 Lagrange equilibrium points in the x, y plane where the star is located at $(-\mu, 0)$, and the planet at $(1-\mu, 0)$. The first three points L_1, L_2, L_3 lie on the x axis and are unstable. The last two equilibrium points L_4, L_5 are $(\frac{1}{2} - \mu, \pm\frac{\sqrt{3}}{2})$ so that the three bodies are the vertices of an equilateral triangle. Though these points are linearly stable they are not Lyapunov stable [22]. Indeed in the normal coordinates the quadratic component of the Hamiltonian reads reads

$$H_2 = \frac{\omega_1}{2}(X^2 + P_x^2) + \frac{\omega_2}{2}(Y^2 + P_y^2) \tag{4}$$

where $\omega_1\omega_2 < 0$ so that the linear motion is quasi-periodic but H_2 has a saddle. From KAM theorem [23] we know that close to L_4 or L_5 most of the orbits are quasi-periodic (their complement has a small measure) and since the corresponding 2D tori are topological barriers to diffusion on the constant energy manifold (the co-dimension is 1) the stability is insured.

The Hénon-Heiles Hamiltonian describes the motion of a star in an elliptical galaxy and its Hamiltonian reads

$$H = T + V = \frac{1}{2}(p_x^2 + p_y^2) + \frac{1}{2}(x^2 + y^2) - \frac{x^3}{3} + xy^2 \tag{5}$$

The potential $V(x, y)$ has a minimum at the origin and three saddle points at $(1, 0)$, $\left(-\frac{1}{2}, \pm\frac{\sqrt{3}}{2}\right)$ where $V = 1/6$. The straight lines defined by

$$V(x, y) - \frac{1}{6} = \frac{1}{6}(1 + 2x)(3y^2 - (1 - x)^2) = 0 \tag{6}$$

intersect at the saddle points which are located at the vertices of an equilateral triangle within which $V(x, y) < 1/6$. The orbits of H within the surface $H < 1/6$ are bounded, the origin is Lyapunov stable and $H = 1/6$ defines the stability boundary.

2.1. *Poincaré section and stability plots*

The phase portraits for the three-body problem are obtained by projecting on the x, v_x plane the intersections with the $y = 0$, $v_y > 0$ or $y = y_c, v_y > 0$ half hyperplane of the orbits belonging to a given energy surface $H = E$. In the x, v_x plane the allowed region is $v_y^2 = (2E - V_{\text{eff}}\,(x, 0)) - v_x^2 > 0$, its boundary is defined by $v_y = 0$ and the initial point for any orbit has $v_y > 0$. The same procedure is used for the Hénon-Heiles model, choosing the $y = 0, p_y > 0$ section and projecting on the x, p_x phase plane. In the three-body problem for any value of E there are unbounded collisional orbits, whereas in the Hénon-Heiles model all the orbits are bounded for $E < 1/6$. As an alternative to the phase portraits, the Lyapunov error and the reversibility error have been considered. The precise definitions and the analytic results on the asymptotic behavior are given in Sec. 5. An advantage is that we are not restricted to the Poincaré section. Indeed to any initial point in a phase plane, we associate the error calculated at time t. The phase portraits exhibit well known structures only if they are obtained by projecting the intersections with an hyperplane of the orbits belonging to an invariant energy surface. However, if for any point in the (x, p_x) phase plane we choose the initial condition by imposing $y = p_y = 0$ (or any other constant value), and project on this plane the corresponding orbits when they intersect the $y = 0$ hyperplane on x, p_x plane, no recognizable patterns are observed since the orbits have different energies. On the contrary, the error plots on the phase plane x, p_x exhibit a very clear pattern connected to the stability of the orbits. In this way, the regions of regular and chaotic motion can be easily discriminated.

For the three-body problem we compare in Fig. 1 the Lyapunov and reversibility error in the x, p_x phase plane near to L_4 choosing $y = 0$, $p_y > 0$ and $H = E = E_c + 10^{-5}$ where E_c is the energy at L_4. The red lines delimiting the accessible area are close to arcs of the hyperbola $p_x^2/2 - (y - y_c)^2\,\alpha/2 = E - E_c$ where $\alpha = -V_{xx}(x_c, 0) > 0$ obtained from $p_y = 0$ with a quadratic approximation to $V(x, 0)$. The blue regions are stable and the corresponding orbits are quasi-periodic, the remaining region corresponds to unbounded and collisional orbits. For the Hénon Heiles Hamiltonian in Fig. 2 we show the REM plots in the (x, p_x) phase plane, choosing $y = 0$ and $H(x, p_x, 0, p_y) = E =$ with $p_y > 0$ for two values of E. These plots exhibit a very close correspondence with the orbits of the Poincaré map. The purple curve delimits the accessible area $p_y^2 \geq 0$ and its boundary is $p_x^2 - 2(E - V(x, 0) = 0$ Almost all the trajectories are chaotic since the chosen energy is at the border of the stability interval. In Fig. 3 we show the reversibility error plot in the (x, p_x) plane having fixed $y = p_y = 0$ for the initial conditions. The stability boundary $H(x, p_x, 0, 0) = 1/6$, purple curve, is the same as in Fig. 2, left panel. The origin is stable and in its neighborhood all the orbits are regular. By approaching the stability boundary the energy increases up to the value $E = 1/6$ and the error grows by several orders of magnitude since the orbits become progressively chaotic.

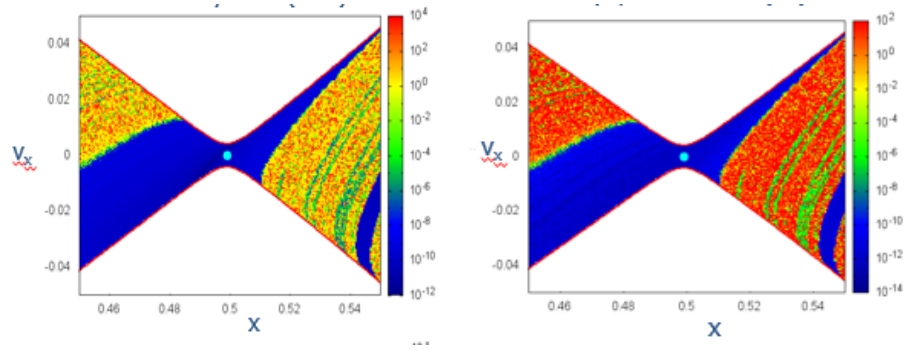

Fig. 1. *REM and LE plots.* Left panel: the reversibility error due to round-off for the three-body problem for $t = 200\,T$ where $T = 2\pi$ is the period. The evolution is based on a fourth order symplectic integrator with time step $\Delta t = T/1000$. A color scale is used for the initial points in a regular grid of (x, v_x) phase plane with $y = 0$, $v_y > 0$ such that $H = E_c + 10^{-5}$. Right panel: the same plot for the Lyapunov error.

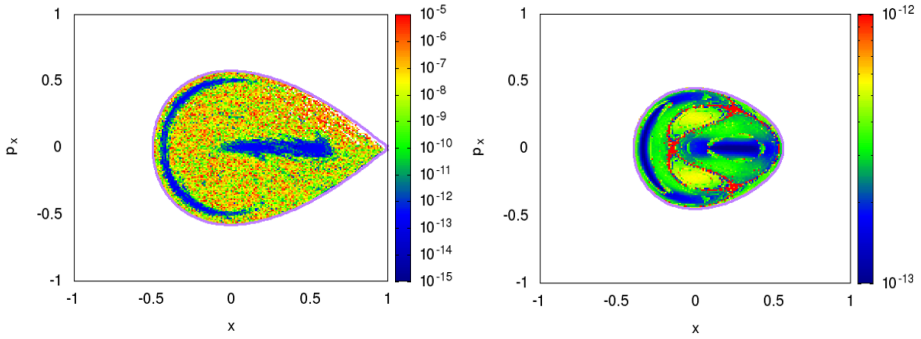

Fig. 2. *REM plot.* Left panel: reversibility error due to round-off for the Hénon-Heiles Hamiltonian at $t = 20T$ where $T = 2\pi$ is the period. The evolution is based on a fourth order symplectic integrator with time step $\Delta t = T/1000$. The initial points are on the (x, p_x) plane with $y = 0$, $p_y > 0$ and $H = 1/6$. The purple curve delimits the accessible region. Right panel: the same plot for $H = 1/10$. The phase portraits for the Poincaré map exhibit a similar structure.

Beyond the boundary the orbits escape to infinity exponentially fast. For initial values $y = p_y = 0.2$ the stability boundary $H(x, p_x, 0.2, 0.2) = 1/6$, purple curve, is narrower, the error increases by approaching it and the transition from regular to chaotic orbits occurs.

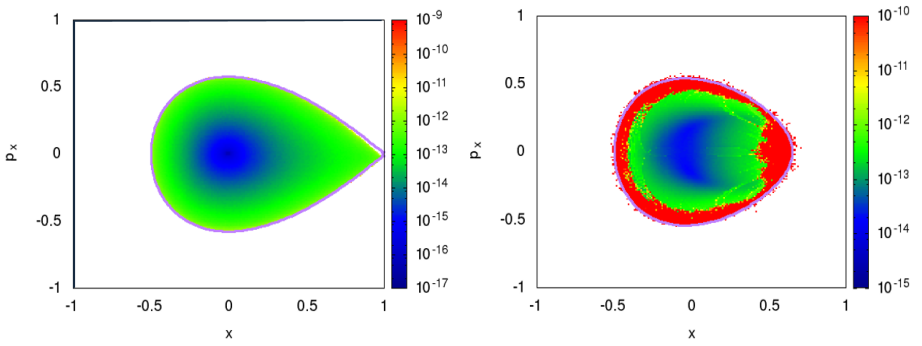

Fig. 3. *REM color map.* Left panel: reversibility error due to round-off for the Hénon-Heiles Hamiltonian at $t = 20T$ with the same integrator as in Fig. 2. The initial points are on the (x, p_x) plane with $y = 0$, $p_y = 0$. The purple curve delimits the stability region. Right panel: the same plot for initial conditions $y = p_y = 0.2$

3. Beam dynamics models and normal forms

Unlikely the Kepler problem the circular motion of a charge under a uniform magnetic field $\mathbf{B}_0 = B_0\,\mathbf{y}$ is not stable since a non zero component of the initial speed along the field causes a drift along it. We assume the quadrupoles, which focus the protons on the reference orbit, to be piecewise constant, and that higher multipoles are thin so that the kick approximation may be used. For a circular ring of radius R the Hamiltonian is

$$H = \frac{p_x^2}{2} + \frac{p_y^2}{2} + \frac{1}{2}\frac{x^2}{R^2} + V(x, y, s) \tag{7}$$

where $s = v_0\, t$ for a speed v_0 along the reference orbit, and $p_x = dx/ds,\ p_y = dy/ds$. The radius is $R = mc\, v_0\gamma/eB_0$ and V is the sum of multi-polar contributions

$$V = -\frac{1}{2}\,K_1(s)(x^2 - y^2) - \frac{1}{6}K_2(s)(x^3 - 3xy^2) + \dots \tag{8}$$

For a real ring the bending magnets alternate with straight sections and R is replaced by the radius of curvature $\rho(s)$. Consider first the linear lattice of length L and compute the one turn map by composing the maps for the straight sections, focusing and de-focusing quadrupoles. Referring for simplicity to a flat beam $y = p_y = 0$ the map is $M(\mathbf{x}) = \mathsf{L}\,\mathbf{x}$ where $\mathbf{x} = (x, p_x)^T$. The matrix L is symplectic namely $\det \mathsf{L} = 1$ so that its eigenvalues are determined by its trace. If $|\mathrm{Tr}(\mathsf{L})| < 2$ the eigenvalues are $e^{\pm i\omega}$, and the map is conjugated to a rotation. The conjugation matrix V can be chosen such that $\mathsf{V}_{12} = 0$ and is represented by

$$\mathsf{L} = \mathsf{V}\mathsf{R}(\omega)\,\mathsf{V}^{-1} \qquad \mathsf{V} = \begin{pmatrix} \beta^{1/2} & 0 \\ -\alpha\beta^{-1/2} & \beta^{-1/2} \end{pmatrix} \qquad \begin{pmatrix} x' \\ p_x' \end{pmatrix} = \mathsf{V}^{-1} \begin{pmatrix} x \\ p_x \end{pmatrix} \tag{9}$$

The matrix L changes whith the section whereas $\mathsf{R}(\omega)$ does not. The functions $\alpha(s)$, $\beta(s)$ define the transformation to the Courant-Sneider coordinates (x', p'_x). The algebraic procedure allows to compute them exactly at any section. The one turn map $\mathsf{L}(s)$ at any other section s is given by

$$\mathsf{L}(s) = \mathsf{A}\,\mathsf{L}(0)\mathsf{A}^{-1} \tag{10}$$

where A denotes the transfer map from 0 to s The ring can be split into a sequence of arcs $[s_{k-1}, s_k]$ with transfer map A_k for $1 \le k \le N$ each one corresponding to a defined magnetic element. Then $\mathsf{L}(s_k) = \mathsf{A}_k\,\mathsf{L}(s_{k-1})\mathsf{A}_k^{-1}$ and $\alpha(s_k), \beta(s_k)$ can be computed by a recurrence relation[24]. A recurrence allows also to compute the phase advance $\Phi(s_k) = \int_0^{s_k} \beta^{-1}(s)\,ds$.

3.1. *The Hénon map models*

The simplest model of a non-linear lattice is given by a linear lattice with a thin sextupole. If the sextupole strength is K_2 and its length is ℓ in the limit $\ell \to 0$ with $\ell K_2 = k_2$ constant its contribution to the potential V is $-\frac{1}{6}\,\delta(s)\,k_2(x^3 - 3xy^2)$ so that the one turn map at $s = 0$ is $M(\mathbf{x})$ and the orbit is recursively given by $\mathbf{x}_{n+1} = M(\mathbf{x}_n)$ where

$$\begin{pmatrix} x_{n+1} \\ \\ p_{x\,n+1} \end{pmatrix} = \mathsf{L} \begin{pmatrix} x_n \\ \\ p_{x\,n} + \frac{1}{2}\,k_2\,x_n^2 \end{pmatrix} \tag{11}$$

Taking into account that $\mathsf{L} = \mathsf{V}\mathsf{R}(\omega\,\mathsf{V}^{-1}$ and scaling the coordinates according to $\mathbf{x}' = \frac{1}{2}\beta_x^{3/2}\,k_2\,\mathsf{V}^{-1}\mathbf{x}$ we obtain the 2D Hénon map

$$\begin{pmatrix} x'_{n+1} \\ \\ p'_{x\,n+1} \end{pmatrix} = \mathsf{R}(\omega) \begin{pmatrix} x'_n \\ \\ p'_{x\,n} + {x'_n}^2 \end{pmatrix}. \tag{12}$$

In the general case we have a 4D map M and the recurrence

$$\begin{pmatrix} x_{n+1} \\ \\ p_{x\,n+1} \\ \\ y_{n+1} \\ \\ p_{y\,n+1} \end{pmatrix} = \begin{pmatrix} \mathsf{L}_x & 0 \\ \\ 0 & \mathsf{L}_y \end{pmatrix} \begin{pmatrix} \mathsf{R}(\omega_x) & 0 \\ \\ 0 & \mathsf{R}(\omega_y) \end{pmatrix} \begin{pmatrix} \mathsf{L}_x^{-1} & 0 \\ \\ 0 & \mathsf{L}_y^{-1} \end{pmatrix} \begin{pmatrix} x_n \\ \\ p_{x\,n} + \frac{k_2}{2}(x_n^2 - y_n^2) \\ \\ y_n \\ \\ p_{y\,n} - k_2 x_n y_n \end{pmatrix}. \tag{13}$$

After the same scaling as in the 2D case $\mathbf{x}' = \frac{1}{2}\beta_x^{3/2}\, k_2\, \mathsf{V}^{-1}\mathbf{x}$ where $\mathsf{V} = \mathsf{V}_x \oplus \mathsf{V}_y$ and defining $\beta = \beta_y/\beta_x$ the map reads

$$\begin{pmatrix} x'_{n+1} \\ p'_{x\,n+1} \\ y'_{n+1} \\ p'_{y\,n+1} \end{pmatrix} = \begin{pmatrix} \mathsf{R}(\omega_x) & 0 \\ & \\ 0 & \mathsf{R}(\omega_y) \end{pmatrix} \begin{pmatrix} x'_n \\ p'_{x\,n} + {x'_n}^2 - \beta {y'_n}^2 \\ y'_{n+1} \\ p'_{y\,n+1} - 2\beta x'_n\, y'_n \end{pmatrix} \tag{14}$$

3.2. *The normal forms*

The non-linear normal forms are the natural extension of the Courant-Sneider theory for a non-linear symplectic one turn map. Referring to the 2D case we write the one turn map in Courant-Sneider coordinates as

$$M(\mathbf{x}') = M_N(\mathbf{x}') + Q_N(\mathbf{x}') \qquad M_N(\mathbf{x}') = \mathsf{R}(\omega)(\mathbf{x}' + P_2(\mathbf{x}') + \ldots + P_N(\mathbf{x}')) \tag{15}$$

where P_k are homogeneous polynomials of order k and Q_N is a remainder. For the Hénon map $M = M_2$ but for a realistic lattice M is a polynomial of very high degree, precisely 2^m if m is the number of sextupoles. The normal form is a representation of the map in a coordinates system where it is explicitly invariant with respect to a continuous or discrete symmetry group. Consider the group generated by $\mathsf{R}(\omega)$: it is continuous if $\omega/2\pi$ is irrational, it is discrete and has only q elements if $\omega/2\pi = m/q$ where m and q are two prime integers. We look for a symplectic change of coordinates $\mathbf{x}' = \Phi(\mathbf{X})$ such that the map is changed into a new one $U(\mathbf{X})$ having the prescribed symmetry. The functional equation which determines Φ and U is

$$M \circ \Phi(\mathbf{X}) = \Phi \circ U(\mathbf{X}). \tag{16}$$

It can be solved iteratively by expanding Φ and U in a series of homogeneous polynomials or order n in X, P_x. Equivalent forms of the functional equation are

$$M(\mathbf{x}') = \Phi \circ U \circ \Phi^{-1}(\mathbf{x}') \qquad U(\mathbf{X}) = \Phi^{-1} \circ M \circ \Phi(\mathbf{X}). \tag{17}$$

The map U is written as the linear map generating the group applied to the time one flow of a symmetric Hamiltonian H

$$U(\mathbf{X}) = \mathsf{R}e^{D_H}(\mathbf{X}) \qquad H(\mathsf{R}\mathbf{X}) = H(\mathbf{X}) \qquad U(\mathsf{R}\mathbf{X}) = \mathsf{R}U(\mathbf{X}). \tag{18}$$

The symplectic coordinates change Φ can also be written as the time one flow of a generating function G

$$\Phi(\mathbf{X}) = e^{D_G}\, \mathbf{X} \tag{19}$$

The first functional equation written for Φ and U can be solved formally by expanding these maps into a series of homogeneous polynomials in X, P_x. Here D_G is the Lie derivative namely $D_G f(\mathbf{X}) = [f, G]_{\mathbf{x}}$ is the Poisson bracket and e^{D_G} denotes the corresponding Lie series. When the frequency is non-resonant $\mathsf{R}(\omega)$ generates the continuous rotations group and we set

$$U = \mathsf{R}(\omega)\, e^{D_H} = e^{D_{H_F}} \tag{20}$$

The rotational invariance implies that $H = H(J)$ where $J = \frac{1}{2}(X^2 + P^2)$ is the action. Its flow interpolates the orbits of the map in the system which rotates with the linear frequency ω. The interpolating Hamiltonian in the fixed frame H_F and the corresponding frequency Ω_F are given by

$$H_F = \omega J + H(J) \qquad \Omega_F = \frac{dH_F}{dJ} = \omega + 2J\,\Omega_2 + (2J)^2\,\Omega_4 + \dots \tag{21}$$

since $\mathsf{R}(\omega)\, e^{D_H} = e^{D_{\omega J}}\, e^{D_{H(J)}} = e^{D_{\omega J + H}}$.

In the resonant case $\omega \equiv \omega_R = 2\pi\, m/q$ the group generated by $\mathsf{R}(\omega_R)$ is discrete. The map U and the interpolating Hamiltonian in the rotating system are written as a series of homogeneous polynomials of order n in X, P_x. The use of complex coordinates $z = X - iP_x$ and z^* is convenient to impose the invariance condition. The map U starts with the identity and the first resonant contribution is z^{*q-1} so that for the corresponding Hamiltonian h the first resonant contributions are z^{*q} and z^q, wheres the non-resonant contributions are $(zz*)^m$ with $m \geq 2$. For instance, if $q = 3$ we have $h \propto z^3 + z^{*3}$ and using the action-angle coordinates defined by $X = (2J)^{1/2}\cos(\Theta)$ together with $P_x = -(2J)^{1/2}\sin(\Theta)$ we obtain

$$H = -4J^{3/2}\cos(3\Theta). \tag{22}$$

The general form of the interpolating Hamiltonian is

$$H = \sum_{k \geq 1} h_k(J)\, \cos(k\, q\, \Theta + \alpha_k). \tag{23}$$

When the frequency ω is close to a resonance $\omega = \omega_R + \epsilon$ we can impose that the map U is invariant with respect to the discrete group generated by $\mathsf{R}(\omega_R)$ and we write $U = \mathsf{R}(\omega_R) e^{D_H}$. The invariance of the map U is insured by the invariance of H. In this case, the map $\mathsf{R}(-\omega_R)\, U$ is no longer tangent to the identity but has a linear term $\mathsf{R}(\epsilon)\mathbf{X}$. As a consequence, the Hamiltonian H has a non-vanishing quadratic component $H = \epsilon J + \dots$. The expansion looks the same as in the resonant case, but the coefficients now depend on ϵ and for $\epsilon \to 0$ the Hamiltonian for the resonant case is recovered. For a resonance of order q the interpolating Hamiltonian can be approximated by

$$H = \epsilon J + \frac{\Omega_2}{2} J^2 + A J^{q/2}\, \cos(q\Theta + \alpha) \tag{24}$$

and exhibits a chain of q islands whose distance from the origin and width vanish as $\epsilon \to 0$.

3.3. *Nekhoroshev estimates*

The normal form series diverge. For a rigorous formulation, the series are truncated at arbitrary order and a remainder is introduced. The functional equation reads

$$M \circ \Phi_N(\mathbf{X}) = \Phi_N \circ (U_N(\mathbf{X}) + E_N(\mathbf{X})), \tag{25}$$

where U_N and Φ_N are first recursively determined starting form the truncated map M_N as a sum of homogeneous polynomials up to order N and E_N is the remainder of order $N+1$. The next step is to replace U_N with a symplectic map having the same polynomial expansion up to order N. This is crucial since this map must be iterated. The coordinates transformation is performed once and eventually one can replace it with a symplectic one

$$U_N = \mathsf{R}(\omega) e^{D_{H_N}} \qquad\qquad \Phi_N = e^{D_{G_N}}. \tag{26}$$

The Hamiltonian H_N is the sum of homogeneous polynomials up to order $N+1$ which are recursively determined starting from U_N first obtained as a polynomial of order N. In the non-resonant case we have $U_N = \mathsf{R}(\Omega_N(\frac{1}{2}(X^2+P_x^2))$ and letting $r = (X^2+P_x^2) = (2J)^{1/2}$ the following estimate holds for the remainder

$$\|E_{N-1}\| \le A \left(\frac{r}{r_N}\right)^N \qquad\qquad r < r_N = \frac{1}{C\,N}. \tag{27}$$

For r fixed the minimum in is achieved for $N = N_* = 1/(Cer)$ so that $r/r_N = e^{-1}$. In a disc of radius r the minimum remainder is bounded by

$$\|E_{N_*}\| \le A\, e^{-N_*} = A\, e^{-r_*/r} \qquad\qquad r_* = \frac{1}{e\,C}. \tag{28}$$

Any orbit with initial point in a disc of radius $r/2$ will remain in a disc of radius r for a number of iterations n exponentially high in $1/r$

$$n < \frac{1}{2}\, A r\, e^{r_*/r}. \tag{29}$$

The Birkhoff series in the non-resonant case diverge due to an accumulation at the origin of the complex $\rho = 2J$ plane of singularities associated to the resonances. If $\omega = 2\pi\, m/q + \epsilon$ for $\epsilon \to 0$, the conjugation function Φ behaves as a geometric series with a pole at $\rho = -\epsilon/\Omega_2$ where the frequency $\Omega \simeq \omega + \Omega_2 \rho$ is resonant. In the generic case when ρ is varied, the frequency crosses infinitely many resonances. The leading ones correspond to the continued fraction expansion m_j/q_j of the tune ν and are located approximately at $\rho_j \simeq -\epsilon_j/\Omega_2$ where $\epsilon_j = \omega - 2\pi\, m_j/q_j$. A rigorous analysis confirms this picture[25]. If $\rho_j > 0$ we have a true resonance corresponding to a chain of islands, while if $\rho_j < 0$ the resonance is virtual since it corresponds to an imaginary value of the radius $r = \sqrt{\rho}$.

4. Dynamic aperture

The normal forms can be computed also for the symplectic 4D one turn map. In the non-resonant case the interpolating Hamiltonian is a function of the actions J_x, J_y which are just twice the horizontal and vertical emittance ϵ_x, ϵ_y. One immediate application is the calculation of the resonance lines in the action space. To find the working point, the resonance lines are drawn in the linear tunes space. The resonant condition is satisfied when there is an integer vector $\mathbf{q} = (q_x, q_y, m)$ such that $q_x\,\nu_x + q_y\nu_y = m$ and corresponds to a line in the tunes plane. The point where two lines cross is a second order resonance, defined by two linearly independent integer vectors $\mathbf{q}_1, \mathbf{q}_2$. Once the working point is chosen, by fixing the linear tunes far enough from low order resonances, one has to consider the resonances of the non-linear tune. In the action plane (J_x, J_y) one can draw resonance lines which cross at the double resonances. The quadratic approximation in J_x, J_y to H

$$H = 2\pi(\nu_x\,J_x + \nu_y\,J_y) + \frac{2\pi}{2}\,(h_{11}J_x^2 + +2h_{12}\,J_xJ_y + h_{22}\,J_y^2) \tag{30}$$

gives a straight line in the action plane for the resonance $\mathbf{q} = (q_x, q_y, m)$

$$a_x\,J_x + a_y\,J_y = b \tag{31}$$

where $a_x = h_{11}\,q_x + h_{12}q_y$ and $a_y = h_{12}\,q_x + h_{22}q_y$ and $b = m - q_x\,\nu_x - q_y\,\nu_y$.

The normal forms can be used to determine the dynamic aperture close to an unstable resonance. The 2D Hénon map when ω approaches 0 corresponds to a first order symplectic integrator of the Hamiltonian $H = \omega(x^2 + p_x^2)/2 - x^3/3$ with a unit time step. After the scaling $x \to \omega x$, $p_x \to \omega\,p_x$ and $H \to \omega^3 H$ we get

$$H = \frac{1}{2}\,(x^2 + p_x^2) - \frac{x^3}{3} \tag{32}$$

The dynamic aperture given by $p = \pm(1-x)\sqrt{(1+2x)/3}$ is the separatrix of H. Another approximation is obtained from the lowest order non-resonant normal form of order 2. The map U is just the linear map so that $H = \frac{1}{2}\,\omega\,(X^2 + P_x^2)$. The transformation $\mathbf{X} = \Phi^{-1}(\mathbf{x})$, which is a polynomial of order 2, allows to write H in the original coordinates as a polynomial of order 3. After the previous scaling with ω the Hamiltonian reads

$$H = \frac{x^2 + p^2}{2} - A\,\frac{x^3}{3} + B\,xp^2 + \frac{\omega}{2}x^2p \tag{33}$$

The coefficients $A = \frac{3}{8}(\omega\cot(3\omega/2) + \omega\cot(\omega/2))$ and $B = \frac{1}{8}(3\omega\cot(3\omega/2) - \omega\cot(\omega/2))$ have a finite limit $A = 1$ and $B = 0$ for $\omega \to 0$ which agrees with the previous interpolating Hamiltonian.
The Hénon map has an hyperbolic fixed point at $x = \frac{2}{\omega}\tan\frac{\omega}{2}$, $p_x = -\frac{2}{\omega}\tan^2\frac{\omega}{2}$ to be compared with the saddle point $x = 1$, $p_x = 0$ of the Hamiltonian in equation 5 with $y = p_y = 0$ and the saddle point $x = 1 + O(\omega^2), p_x = -\frac{\omega}{2} + O(\omega^3)$ of the Hamiltonian in equation 33. The numerical results confirm the higher accuracy of this estimate.

If $\omega = 2\pi/3 + \epsilon$ we consider the quasi resonant normal form to approximate the dy-

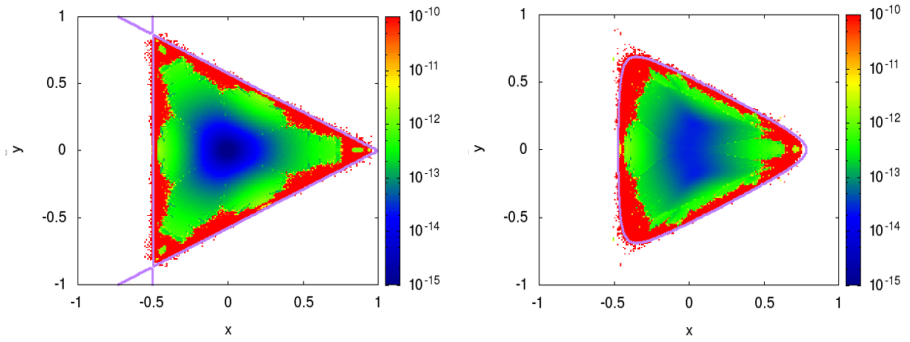

Fig. 4. *REM color map.* Left panel: reversibility error due to round-off for the 4D Hénon map with linear tunes $\nu_x = \nu_y = 0.01$ iterated $n = 5000$ times in the plane x, y with $y = 0$, $p_y = 0$ for the initial conditions. Right panel: the same plot for initial conditions with $p_x = 0.2$, $p_y = 0.2$

namic aperture as $\epsilon \to 0$. The interpolating Hamiltonian is $H = \epsilon J - 4J^{3/2}\cos(3\Theta)$ and written in Cartesian coordinates after the scaling $x \to \epsilon\, x/4$, $p_x \to \epsilon p_x/4$ and $H \to \epsilon^3\, H/16$ reads

$$H = \frac{x^2 + p_x^2}{2} + \frac{3x(x^2 + p_x^2) - 4x^3}{2\sqrt{2}} \tag{34}$$

There are three saddle points at $x = \frac{2\sqrt{2}}{3}$, $p_x = 0$ and $x = -\frac{\sqrt{2}}{3}$, $p_x = \pm\frac{\sqrt{2}}{\sqrt{3}}$ where $H = 4/27$. The Hamiltonian has the same value at the straight lines joining these points so that the equilateral triangle having these points as vertices corresponds to the dynamic aperture as on can prove observing that

$$H - \frac{4}{27} = \frac{1}{2}\left(1 + \frac{3x}{\sqrt{2}}\right)\left(p^2 - \frac{1}{3}\left(x - \frac{2\sqrt{2}}{3}\right)^2\right) \tag{35}$$

Finally we consider the 4D Hénon map with equal frequencies ω close to 0. The interpolating Hamiltonian is the same as the Hénon-Heiles Hamiltonian which has three saddle points at $p_x = p_y = 0$ with $x = 1$, $y = 0$ and $x = -\frac{1}{2}$, $y = \pm\frac{\sqrt{3}}{2}$. As a consequence, the dynamic aperture is a closed 3D surface defined by

$$H - \frac{1}{6} = \frac{p_x^2 + p_y^2}{2} + \frac{1}{6}(1 + 2x)\big(\,3y^2 - (1 - x)^2\,\big) = 0 \tag{36}$$

and the stable region is the interior $H < 1/6$. In Fig. 4 we show in the phase plane x, p_x the reversibility error plot by fixing the remaining two coordinates, in this case, fixing $y_0, p_{y\,0}$. The stable region is given by $H(x, p_x, y_0, p_{y\,0}) \le 1/6$ and this analytic result agrees very well with the dynamic aperture obtained from numerical simulations when $\omega \ll 1$. In Fig. 5 we show the REM error plot for the same 4D Hénon map but in the p_x, p_y momentum plane.

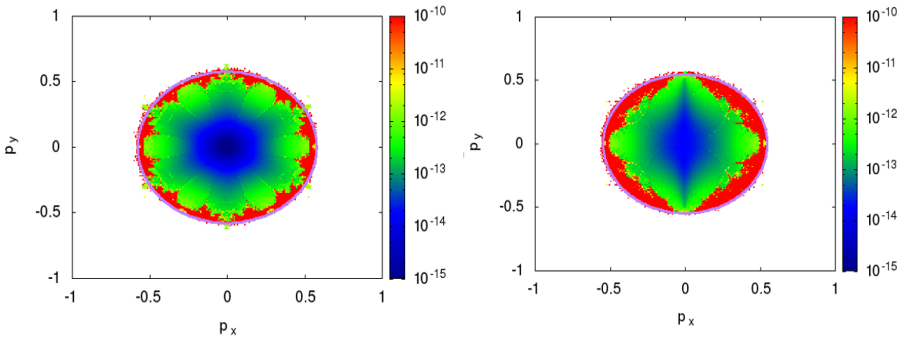

Fig. 5. *REM color map.* Left panel: reversibility error due to round-off for the 4D Hénon map with linear tunes $\nu_x = \nu_y = 0.01$ iterated $n = 5000$ times in the plane p_x, p_y with $x = 0$, $y = 0$ for the initial conditions. Right panel: the same plot for initial conditions with $x = 0.2$, $y = 0.2$

5. Lyapunov and reversibility errors

For a symplectic map the errors due to a small initial displacement or to a small additional noise have well defined asymptotic properties which depend on the nature of the reference orbit. Their use is suggested for the symplectic one turn maps of beam dynamics as an alternative to the error in frequency analysis[26–28]. We recall here the definitions of LE, FE, RE, the algorithms based on tangent map, and the results on their asymptotic growth for linear maps. In addition, by using the normal forms we prove that the growth of errors for a non-linear map follows a power law in the quasi-integrable region.

Lyapunov error

The orbits of a symplectic map $M(\mathbf{x})$ corresponding to initial conditions $\mathbf{x}_0$ and $x_0 + \epsilon\boldsymbol{\eta}_0$ are $\mathbf{x}_n = M^n(\mathbf{x}_0)$ and $\mathbf{x}_{\epsilon,\,n} = M^n(\mathbf{x}_0 + \epsilon\boldsymbol{\eta}_0)$. As a consequence

$$\mathbf{x}_{\epsilon,\,n} = \mathbf{x}_n + \epsilon\,\boldsymbol{\eta}_n + O(\epsilon^2) \qquad\qquad \boldsymbol{\eta}_n = DM(\mathbf{x}_{n-1})\boldsymbol{\eta}_{n-1} \tag{37}$$

$DM(\mathbf{x})$ denotes the Jacobian of the map M. Introducing the matrices $\mathsf{A}_n = DM^n(\mathbf{x}_0)$ we have $\boldsymbol{\eta}_n = \mathsf{A}_n\,\boldsymbol{\eta}_0$ where

$$\mathsf{A}_n = DM(\mathbf{x}_{n-1})\,\mathsf{A}_{n-1} \qquad\qquad \mathsf{A}_0 = \mathsf{I} \tag{38}$$

The Lyapunov error depends on the direction of the initial displacement if it is defined as usually according to

$$e_n^{(L)}(\boldsymbol{\eta}_0) = \|\boldsymbol{\eta}_n\| = \left(\boldsymbol{\eta}_0 \cdot \mathsf{A}_n\,\mathsf{A}_n^T\,\boldsymbol{\eta}_0\right)^{1/2} \tag{39}$$

We choose the following definition of the Lyapunov error

$$e_n^{(L)} = \left(\ \mathrm{Tr}\,(\mathsf{A}_n\mathsf{A}_n^T)\ \right)^{1/2} \tag{40}$$

This error is the quadratic average of the errors on an orthonormal basis $\mathbf{u}_j = \mathsf{R}\mathbf{e}_j$ where $(\mathbf{e}_j)_k = \delta_{j,k}$ and R is a rotation matrix

$$\sum_j \left(e_n^{(L)}(\mathbf{u}_j) \right)^2 = \sum_j \mathbf{e}_j \cdot \mathsf{R}^T \, \mathsf{A}_n \, \mathsf{A}_n^T \, \mathsf{R} \, \boldsymbol{\eta}_j = \mathrm{Tr}\,(\mathsf{R}^T \, \mathsf{A}_n \, \mathsf{A}_n^T \, \mathsf{R}) = \left(e_n^{(L)} \right)^2 \tag{41}$$

We have checked that with this definition the spurious structures for LE[29], due to the choice of the initial vector $\boldsymbol{\eta}_0$, disappear. The maximum Lyapunov exponent is given by

$$\lambda = \lim_{n\to\infty} \frac{1}{n} \log e_n^{(L)}. \tag{42}$$

Forward error

Given a sequence of normalized independent random vectors $\boldsymbol{\xi}_n$

$$\langle\, \boldsymbol{\xi}_n \,\rangle = 0 \qquad \langle\, (\boldsymbol{\xi}_m)_i \, (\boldsymbol{\xi}_n)_j \,\rangle = \delta_{m\,m}\, \delta_{i\,j} \quad \text{or} \quad \langle\, \boldsymbol{\xi}_m \, \boldsymbol{\xi}_n^T \,\rangle = \mathsf{I}\, \delta_{mn} \tag{43}$$

the stochastically perturbed orbit is given by

$$\mathbf{x}_{\epsilon,\,n+1} = M(\mathbf{x}_{\epsilon,\,n}) + \epsilon\, \boldsymbol{\xi}_{n+1} \qquad n \geq 0 \tag{44}$$

The displacement of the noisy orbits from the reference one is

$$\mathbf{x}_{\epsilon,\,n} = \mathbf{x}_n + \epsilon \boldsymbol{\Xi}_n + O(\epsilon^2) \tag{45}$$

where $\boldsymbol{\Xi}_n$ proves to satisfy the linear non homogeneous recurrence

$$\boldsymbol{\Xi}_n = DM(\mathbf{x}_{n-1})\, \boldsymbol{\Xi}_{n-1} + \boldsymbol{\xi}_n \qquad n \geq 1 \qquad \boldsymbol{\xi}_0 = 0 \tag{46}$$

whose solution is

$$\boldsymbol{\Xi}_n = \sum_{k=1}^{n} DM^{n-k}(\mathbf{x}_k)\, \boldsymbol{\xi}_k = \sum_{k=0}^{n-1} \mathsf{B}_k \, \boldsymbol{\xi}_{n-k} \qquad \mathsf{B}_k = DM^k(\mathbf{x}_{n-k}) \tag{47}$$

The matrices B_k satisfies the recurrence

$$\mathsf{B}_k = \mathsf{B}_{k-1}\, DM(x_{n-k}) \qquad k = 1, \ldots, n \qquad \mathsf{B}_0 = \mathsf{I} \tag{48}$$

The covariance matrix of the process $\boldsymbol{\xi}_n$ is

$$\Sigma_n^{2\,(F)} = \langle\, \boldsymbol{\Xi}_n \, \boldsymbol{\Xi}_n^T \,\rangle = \sum_{k=0}^{n-1} \mathsf{B}_k \, \mathsf{B}_k^T, \tag{49}$$

and the forward error (FE) is defined by

$$e_n^{(F)} = \langle\, \boldsymbol{\Xi}_n \cdot \boldsymbol{\Xi}_n \,\rangle^{1/2} = \langle\, \mathrm{Tr}\,(\boldsymbol{\Xi}_n \, \boldsymbol{\Xi}_n^T) \,\rangle^{1/2} \left(\mathrm{Tr}\,(\Sigma_n^{2\,(F)}) \right)^{1/2}. \tag{50}$$

Reversibility error

We consider n forward iterations of the map followed by m iterations of the inverse map with a random error at each step. Let

$$\mathbf{x}_{\epsilon,\,-m,n} = M(\mathbf{x}_{\epsilon,\,-m+1,n}) + \epsilon\boldsymbol{\xi}_{-m} \qquad m \geq 1 \qquad \mathbf{x}_{\epsilon,0,n} = \mathbf{x}_{\epsilon,n} \tag{51}$$

we define the

$$\mathbf{x}_{\epsilon,\,-m,n} = \mathbf{x}_{n-m} + \epsilon\boldsymbol{\Xi}_{-m,n} + O(\epsilon^2) \tag{52}$$

where $\boldsymbol{\Xi}_{-m,n}$ satisfies the recurrence

$$\boldsymbol{\Xi}_{-m,n} = DM(\mathbf{x}_{n-m+1})\boldsymbol{\Xi}_{-m+1,n} + \boldsymbol{\xi}_{-m} \qquad m \geq 1 \qquad \boldsymbol{\Xi}_{0,\,n} = \boldsymbol{\Xi}_n \tag{53}$$

whose solution is

$$\boldsymbol{\Xi}_{-m,n} = DM^{-m}(\mathbf{x}_n)\boldsymbol{\Xi}_n + \sum_{k=1}^{m} DM^{-(m-k)}(\mathbf{x}_{n-k})\boldsymbol{\xi}_{-k} \tag{54}$$

The deviation from the initial condition $\mathbf{x}_{\epsilon,-n,n} - \mathbf{x}_0$ is a stochastic process defined by

$$\boldsymbol{\Xi}_n^{(R)} = \boldsymbol{\Xi}_{-n,n} = DM^{-n}(\mathbf{x}_n)\ \boldsymbol{\Xi}_n + \sum_{k=1}^{n} DM^{-(n-k)}(\mathbf{x}_{n-k})\ \boldsymbol{\xi}_{-k} \tag{55}$$

Defining the matrices

$$\mathsf{A^I}_k = DM^{-k}(\mathbf{x}_k) \qquad \mathsf{C}_k = \mathsf{A^I}_n\,\mathsf{B}_k \tag{56}$$

which can be computed with the recurrence

$$\mathsf{A^I}_k = \mathsf{A^I}_{k-1}\,DM^{-1}(\mathbf{x}_k) \qquad k \geq 1 \qquad \mathsf{A^I}_0 = \mathsf{I} \tag{57}$$

we can write

$$\boldsymbol{\Xi}_n^{(R)} = \sum_{k=0}^{n-1}\ \mathsf{C}_k\ \boldsymbol{\xi}_k + \sum_{k=0}^{n-1} \mathsf{A^I}_k\ \boldsymbol{\xi}_{-(n-k)} \tag{58}$$

The covariance matrix is

$$\Sigma_n^{(R)} = \langle\, \boldsymbol{\Xi}_n^{(R)}\, (\boldsymbol{\Xi}_n^{(R)})^T \,\rangle = \sum_{k=0}^{n-1} \mathsf{C}_k\mathsf{C}_k^T \ + \ \sum_{k=0}^{n-1} \mathsf{A^I}_k\, \mathsf{A^I}_k^T \tag{59}$$

and the reversibility error is defined by

$$e_n^{(R)} = \langle\, \boldsymbol{\Xi}_n^{(R)} \cdot \boldsymbol{\Xi}_n^{(R)} \,\rangle^{1/2} = \Big(\,\mathrm{Tr}\,\big(\Sigma_n^{2\,(R)}\big)\,\Big)^{1/2}. \tag{60}$$

Linear maps

In the case of a linear map $DM(\mathbf{x}) = \mathsf{A}$ the errors can be easily compared. Indeed in this case $\mathsf{A}_k = \mathsf{A}^k$, $\mathsf{B}_k = \mathsf{A}^k$ and $\mathsf{A^I}_k = \mathsf{A}^{-k}$, $\mathsf{C}_k = \mathsf{A}^{-(n-k)}$ As a consequence

$$\big(\,e_n^{(L)}\big)^2 = \ \mathrm{Tr}\,\big(\mathsf{A}^n\,(\mathsf{A}^n)^T\,\big) \qquad \big(\,e_n^{(F)}\big)^2 = \sum_{k=0}^{n-1} \big(\,e_k^{(L)}\big)^2 \tag{61}$$

For the reversibility error we have

$$\left(e_n^{(R)}\right)^2 = 2\sum_{k=0}^{n-1} \mathrm{Tr}\left(\mathsf{A}^{-k}\left(\mathsf{A}^{-k}\right)^T\right) + \mathrm{Tr}\left(\mathsf{A}^{-n}\left(\mathsf{A}^{-n}\right)^T - \mathsf{I}\right) \tag{62}$$

Letting Λ be the normal form $\mathsf{A} = \mathsf{U}\Lambda\mathsf{U}^{-1}$ we have $\mathrm{Tr}\left(\mathsf{A}^k\left(\mathsf{A}^k\right)^T\right) = \mathrm{Tr}\left(\mathsf{V}\Lambda^k\mathsf{V}^{-1}\left(\Lambda^k\right)^T\right)$ where $\mathsf{V} = \mathsf{U}^T\mathsf{U}$ is symmetric. In dimension 2 we can easily prove that $\mathrm{Tr}\left(\mathsf{A}^k\left(\mathsf{A}_k\right)^T\right) = \mathrm{Tr}\left(\mathsf{A}^{-k}\left(\mathsf{A}^{-k}\right)^T\right)$ so that

$$\left(e_n^{(R)}\right)^2 = 2\left(e_n^{(F)}\right)^2 + \left(e_n^{(L)}\right)^2 - 2 \tag{63}$$

The stability and errors growth rate depend on the linear matrix A and the following classification holds in the 2D case

If $\mathrm{Tr}\left(\mathsf{A}\right)| > 2$ then $\Lambda = \mathrm{diag}(e^{\lambda}, e^{-\lambda})$ and all errors grow exponentially $e_n \sim e^{n\lambda}$.

If $\mathrm{Tr}\left(\mathsf{A}\right)| < 2$ the normal form is a rotation $\Lambda = \mathsf{R}(\omega)$ and e_n^L is bounded whereas $e_n^{(F)}$, $e_n^{(R)}$ grow as $n^{1/2}$ with oscillations. Indeed $\left(e_n^{(L)}\right)^2 = C + (C-2)\cos(2n\omega)$ where $C \geq 2$. If $\mathsf{A} = \mathsf{R}(\omega)$ then $C = 2$ so that $e_n^{(F)} = \sqrt{2n}$ and $e_n^{(R)} = \sqrt{4n} = e_{2n}^{(F)}$

If $\mathrm{Tr}\left(\mathsf{A}\right)| = 2$ the normal form is a Jordan form $\Lambda = \begin{pmatrix} 0 & \alpha \\ 0 & 1 \end{pmatrix}$ and in this case e_n^L grows as n whereas $e_n^{(F)}$, $e_n^{(R)}$ grow as $n^{3/2}$

Integrable and quasi integrable maps

The map in the integrable case reads

$$M(\mathbf{x}) = \mathsf{R}(\Omega(J))\mathbf{x} \qquad\qquad J = \frac{\|\mathbf{x}\|^2}{2} \tag{64}$$

where J is is an invariant. The tangent map to M^n is is

$$DM^n(\mathbf{x}) = \mathsf{R}(n\Omega(J)) + n\,\Omega'(J)\,\mathsf{R}'(n\Omega(J))\,\mathbf{x}\mathbf{x}^T \tag{65}$$

The Lyapunov error is given by

$$\left(e_n^{(L)}\right)^2 = \mathrm{Tr}\left[\left(\mathsf{R}^T(n\Omega)+n\Omega'\mathbf{x}\mathbf{x}^T\,\mathsf{R}'^T(n\Omega)\right)\left(\mathsf{R}(n\Omega)+n\Omega'\mathsf{R}'(n\Omega)\mathbf{x}\mathbf{x}^T\right)\right] = 2+n^2\,\Omega'^2\,\|\mathbf{x}\|^4 \tag{66}$$

where we have taken into account $\mathsf{R}^T\mathsf{R}' = \mathsf{J}$ and $\mathsf{R}'^T\mathsf{R}' = \mathsf{I}$. As a consequence setting $\alpha = \Omega'\|\mathbf{x}\|^2 = 2J\Omega'$ we can write

$$\left(e_n^{(L)}\right)^2 = 2+\alpha^2 n^2\,\|\mathbf{x}\|^4 \qquad \left(e_n^{(F)}\right)^2 = \sum_{k=0}^{n-1}\left(e_n^{(L)}\right)^2 = 2n+\alpha^2\left(\frac{n^3}{3}-\frac{n^2}{2}+\frac{n}{6}\right)\|\mathbf{x}\|^4. \tag{67}$$

For the reversibility error we find

$$\left(e_n^{(R)}\right)^2 = 4n + \alpha^2\,\|\mathbf{x}\|^4 \sum_{k=1}^{2n-1} k^2 = \left(e_{2n}^{(F)}\right)^2. \tag{68}$$

For a generic polynomial map, such as the map with a non-resonant linear frequency we can use the normal form representation and, in a disc of sufficiently small radius r, we can neglect the remainder since it can be made exponentially small. As a consequence, we write $M = \Phi \circ \mathsf{R}(\omega) \circ \Phi^{-1}$

$$e_L^2(n) = \mathrm{Tr}\left[\mathsf{B}\,(DR(n\Omega))^T\,\mathsf{A}\,DR(n\Omega)\right] \tag{69}$$

where

$$\mathsf{B} = D\Phi^{-1}(\mathbf{x}_0)\,(D\Phi^{-1}(\mathbf{x}_0))^T \qquad \mathsf{A} = [D\Phi(R(n\Omega))^T\,D\Phi(R(n\Omega))]. \tag{70}$$

Since Φ is a symplectic transformation, A and B are positive symplectic matrices and $e_L^2(n) = a(n) + n\,b(n) + n^2\,c(n)$ where the coefficients are bounded and oscillating. As a consequence, $e_L(n)$ grows as αn with oscillations wheres $e_F(n)$ and $e_R(n)$ grow as $\alpha n^{3/2}$ with oscillations.

Using the quasi-resonant normal forms one can consider the case in which we are close to a resonance. Within any island one can use the non-resonant normal forms for its elliptic point. Finally the same estimates hold. By approaching the separatrix the frequency vanishes as $1/\log|J - J_s|$ where the action has a different expression before and within the island. In any case a power law is always observed with a coefficient α with diverges on the separatrix itself. The non-integrability effects due to the neglected remainder change the separatrix into a thin chaotic layer where the error has an exponential growth.

5.1. *Numerical results for the Hénon maps*

We propose a stability analysis based on the errors previously defined. The numerical results confirm the theoretical predictions, a power law growth for regular orbits, an exponential growth for chaotic orbits. In order to kill the oscillations on the regular orbits an averaging procedure has been proposed. Let $e(n)$ be an interpolation of the error such that $e(n) = e_n$ for n integer and let

$$De(n) = \frac{d\log e(n)}{d\log n} = n\frac{d\log e(n)}{dn} \tag{71}$$

For a power law $e(n) = n^\gamma$ we have $D\,e(n) = \gamma$ whereas for an exponential law $e(n) = e^{\lambda n}$ we have $D\,e(n) = n\lambda$. The following double average with respect to n was proposed

$$Y(n) = \langle\,\langle\,De(n)\,\rangle\,\rangle \tag{72}$$

where $Y(n)$ is the mean exponential growth factor of nearby orbits (MEGNO) [14,15]. The growth with n of the errors $e(n)$ and their MEGNO averages $Y(n)$ is shown in Fig. 6 for a regular orbit of the Hénon map. The exact expressions based on the tangent map are used to compute LE, FE, RE. We have also considered the reversibility error (REM) due to the round-off. The amplitude of oscillations for RE is much smaller with respect to FE. For a rotation with constant frequency,

REM grows as n whereas RE grows as $n^{1/2}$. For an anisochronous rotation (the frequency depends on action) REM grows as n^2 whereas RE grows as $n^{3/2}$, but within a tiny chain of islands both grow as $n^{3/2}$. In Fig. 7 we show how the errors vary when we move along a line crossing an island in the x, p_x phase plane. The error increases reaching a maximum on the pseudo-separatrix. A magnification around it shows that MEGNO does not reach a constant value but has a linear growth. We have repeated the computation with the resonant normal form which has a chain of islands with a real separatrix and in this case MEGNO never exceeds the value 1/2 for LE and 3/2 for FE and RE. Within the island REM and RE are very close and the power law exponent is the same (see Fig. 7).

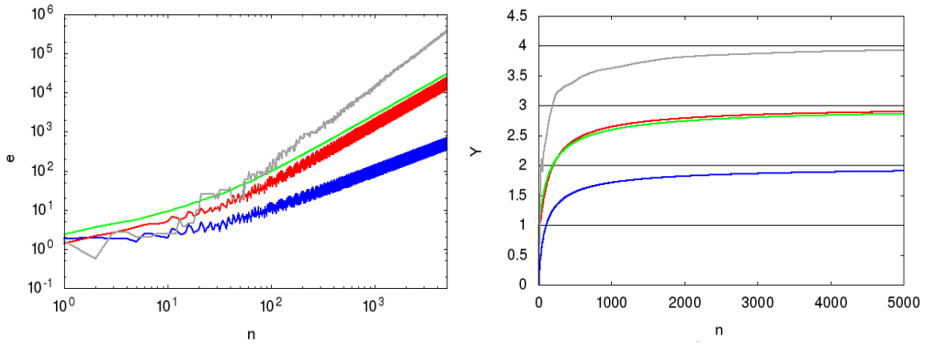

Fig. 6. Left panel: comparison in a log-log scale of the errors $e(n)$ when n is varied for an orbit of the Hénon map with $\nu = 0.21$ and $x_0 = 0.76, p_0 = 0$. LE (blue line), FE (red line), RE (green line) and REM (grey line). Right panel: the same for the MEGNO average Y(n)

In Fig. 8 we compare the errors in the phase plane for a fixed value of n excluding the unstable points which are beyond the dynamic aperture. The pictures are very similar and suggest that the computation of just LE and REM is adequate. We have compared the LE and REM errors with the error performed with the frequency analysis, defined as the error on the frequency computed on one orbit of length $n = 2^{m-1}$ and $n = 2^m$. The main feature is that the variation along a line in the phase space joining the origin with the center of an island is much less regular unless a very long orbit is computed (typically $n = 2^{14}$).

Some spikes, whose origin is numerical rather dynamical, are observed and they are not present in REM. Similar considerations hold for the error plots in the phase space. For the 4D Hénon map we have examined a large number of error plots in a phase plane, fixing the remaining two coordinates. Usually values of n below 1000 are sufficient. It is possible to have a tree dimensional view of the errors by

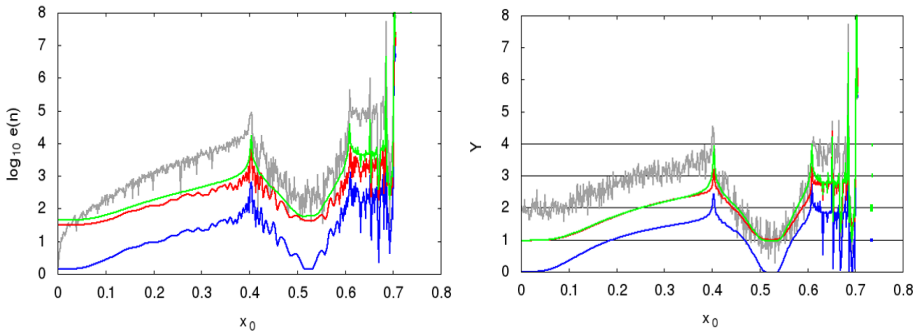

Fig. 7. Left panel: comparison the errors $e(n)$ for the Hénon map with $\nu = 0.21$ when the initial point (x_0, p_{x0}) is varied along the line joining the origin with the center of the first island in the $x > 0$, $p_x > 0$ sector. LE (blue line), FE (red line), RE (green line) and REM (grey line). Right panel: the same for the MEGNO average Y(n)

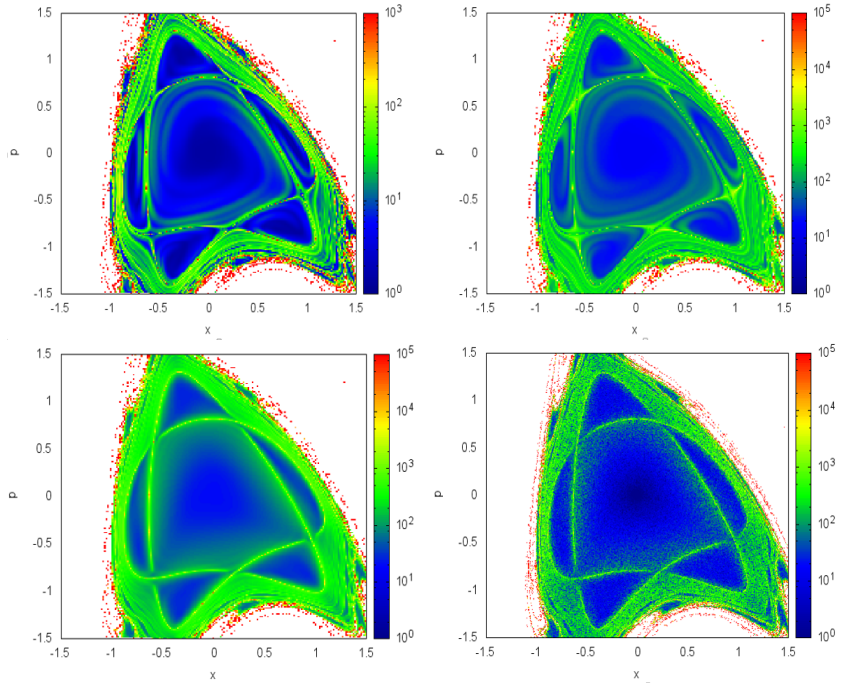

Fig. 8. Comparison the errors $e(n)$ for $n = 100$ and initial points on a grid of the x, p_x phase plane for the 2D Hénon map with $\nu = \sqrt{2} - 1$. Upper left Lyapunov error, upper right forward error, lower left reversibility error, lower right reversibility error due to round-off.

fixing just one coordinate say p_y, drawing in x, p_x plane the error plot with a color scale and varying y step by step until the dynamic aperture shrinks to zero. The animation on a grid 200×200 with a few tenths of values of y which lasts about

one minute allows to have a reliable stability portrait of this 3D subspace. A few animations corresponding to different values of p_y complete the stability picture. The required CPU-time is low since a single 2D plot takes a few minutes and an animation about one hour on a single processor. For a better understanding of the long term dynamic aperture one might compare the maximum distance reached in the phase space with the corresponding LE or REM errors. Since in this case the number of iterations is considerably higher, a cluster of processors is needed.

6. Conclusions

Celestial and beam dynamics have the same Hamiltonian structure and many common features concerning the stability problem. For this reason methods first developed in celestial mechanics, such as canonical perturbation theory, have been exported to beam dynamics. The Birkhoff normal forms are the version of perturbation theory suited to analyze the topology of orbits and the stability of symplectic maps. Their use was proposed for the one turn map of a circular accelerator as the natural generalization of the Courant-Sneider theory. The frequency map analysis first proposed for the planetary motion was applied to the one turn map on a ring. We have examined the analogies between two basic models in celestial mechanics, the three-body problem and the Hénon Heiles Hamiltonian, and two beam dynamics models such as the 2D and 4D Hénon maps. For a Hamiltonian with 2 degrees of freedom the Poincaré section method allows to visualize the orbits belonging to a constant energy surface. For a Hamiltonian with 3 degrees of freedom it is no longer possible to visualize the orbits unless we have an additional integral of motion. The orbits of a 4D symplectic map, can be conveniently visualized only if we know an invariant of motion. This problem was overcome in celestial mechanics by using the Lyapunov error and more recently the reversibility error a stability indicator. The frequency error method requires long orbits which can trigger numerical instabilities, but the Lyapunov and reversibility errors do not face these problems. The error depends only on the initial conditions and the number of iterations. As a consequence one can choose two coordinates in a given phase plane and fix the remaining ones (no invariant manifold is needed). This is a common procedure for models with many degrees of freedom such as a planetary system where the phase plane coordinates are, for instance, the semi-major axis and the eccentricity of a planet. In the restricted three-body problem, one can choose the x, y coordinates of the satellite fixing its initial velocity.
The error plot in the chosen phase plane allows to discriminate the stability of the orbits. For a symplectic 4D map the error plot in a chosen phase plane is obtained fixing the two remaining coordinates. The Birkhoff normal forms allow to determine the short term dynamic aperture close to the unstable (0,1/3) resonances and to prove the power law growth rate, with a pre-factor proportional to the de-tuning, for the Lyapunov and noise-induced errors for the orbits belonging to invariant tori, which they interpolate. The reversibility error due to round-off REM is a

numerical recipe, for which no rigorous foundation can be established. Nevertheless the stability plots provided by REM and RE are very similar for symplectic maps having a sufficiently high computational complexity and the use of the former is by far faster and easier to implement. As a consequence its use jointly with LE is suggested for the one turn maps even for a deeper investigation of the long term dynamic aperture since their application to the orbital stability of exoplanets have been established quite successfully.

7. Acknowledgements

This work has been supported by Polish National Science Centre MAESTRO grant DEC-2012/06/A/ST9/00276.

References

1. V. Szebehely, *Theory of orbits. The restricted problem of three bodies* 1967.
2. M. Henon and C. Heiles, The applicability of the third integral of motion: Some numerical experiments, *AJ* **69**, p. 73 (February 1964).
3. N. N. Nekhoroshev, An exponential estimate of the time of stability of nearly-integrable hamiltonian systems, *Russian Mathematical Surveys* **32**, p. 1 (1977).
4. A. Bazzani, S. Marmi and G. Turchetti, Nekhoroshev estimate for isochronous non resonant symplectic maps, *Celestial Mechanics and Dynamical Astronomy* **47**, 333 (1990).
5. A. Bazzani, P. Mazzanti, G. Servizi and G. Turchetti, Normal forms for Hamiltonian maps and nonlinear effects in a particle accelerator, *Nuovo Cimento B Serie* **102**, p. 51 (1988).
6. A. Bazzani, E. Todesco, G. Turchetti and G. Servizi, A Normal form approach to the theory of nonlinear betatronic motion, *CERN Yellow Reports* **94-02** (March 1994).
7. A. Bazzani, M. Giovannozzi, G. Servizi, E. Todesco and G. Turchetti, Resonant normal forms, interpolating Hamiltonians and stability analysis of area preserving maps, *Physica D Nonlinear Phenomena* **64**, 66 (April 1993).
8. E. Forest, *Nonlinear Normal Forms*, in *From Tracking Code to Analysis: Generalised Courant-Snyder Theory for Any Accelerator Model*, (Springer Japan, Tokyo, 2016), Tokyo, pp. 121–149.
9. C. Froeschlé, E. Lega and R. Gonczi, Fast Lyapunov Indicators. Application to Asteroidal Motion, *Celestial Mechanics and Dynamical Astronomy* **67**, 41 (January 1997).
10. F. Panichi, L. Ciotti and G. Turchetti, Fidelity and reversibility in the restricted three body problem, *Communications in Nonlinear Science and Numerical Simulation* **35**, 53 (2016).
11. F. Panichi, K. Goździewski and G. Turchetti, The reversibility error method (REM): a new, dynamical fast indicator for planetary dynamics, *MNRAS* **468**, 469 (June 2017).
12. J. Souchay and R. Dvorak (eds.), *The Lyapunov Characteristic Exponents and Their Computation*, Lecture Notes in Physics, Berlin Springer Verlag Vol. 790, March 2010.
13. D. Faranda, M. F. Mestre and G. Turchetti, Analysis of Round off Errors with Reversibility Test as a Dynamical Indicator, *International Journal of Bifurcation and Chaos* **22**, p. 1250215 (September 2012).
14. P. M. Cincotta and C. Simó, Simple tools to study global dynamics in non-axisymmetric galactic potentials - I, *A&AS* **147**, 205 (December 2000).

15. P. M. Cincotta, C. M. Giordano and C. Simó, Phase space structure of multi-dimensional systems by means of the mean exponential growth factor of nearby orbits, *Physica D Nonlinear Phenomena* **182**, 151 (August 2003).
16. K. Goździewski, E. Bois, A. J. Maciejewski and L. Kiseleva-Eggleton, Global dynamics of planetary systems with the MEGNO criterion, *A&A* **378**, 569 (November 2001).
17. T. Y. Galushina and G. E. Sambarov, The dynamical evolution and the force model for asteroid (196256) 2003 EH1, *Planet. Space Sci.* **142**, 38 (August 2017).
18. S. Breiter, B. Melendo, P. Bartczak and I. Wytrzyszczak, Synchronous motion in the Kinoshita problem. Application to satellites and binary asteroids, *A&A* **437**, 753 (July 2005).
19. T. C. Hinse, A. A. Christou, J. L. A. Alvarellos and K. Goździewski, Application of the MEGNO technique to the dynamics of Jovian irregular satellites, *MNRAS* **404**, 837 (May 2010).
20. M. Fouchard, E. Lega, C. Froeschlé and C. Froeschlé, On the Relationship Between Fast Lyapunov Indicator and Periodic Orbits for Continuous Flows, *Celestial Mechanics and Dynamical Astronomy* **83**, 205 (May 2002).
21. C. D. Murray and S. F. Dermott, *Solar system dynamics* 1999.
22. E. Belbruno, *Capture dynamics and chaotic motions in celestial mechanics: with applications to the construction of low energy transfers* (Princeton Univ., Princeton, NJ, 2004).
23. V. I. Arnold, *Mathematical methods of classical mechanics* 1978.
24. F. Bergamini, G. Franchetti and G. Turchetti, The micromaps description of a beam with space charge, *Nuovo Cimento A Serie* **112**, p. 429 (May 1999).
25. A. Bazzani and G. Turchetti, Singularities of normal forms and topology of orbits in area-preserving maps, *Journal of Physics A Mathematical General* **25**, L427 (April 1992).
26. J. Laskar, The chaotic motion of the solar system - A numerical estimate of the size of the chaotic zones, *Icarus* **88**, 266 (December 1990).
27. *Frequency Map Analysis and Particle Accelerators* 2003.
28. Y. Papaphilippou, Detecting chaos in particle accelerators through the frequency map analysis method, *Chaos* **24**, p. 024412 (June 2014).
29. R. Barrio, W. Borczyk and S. Breiter, Spurious structures in chaos indicators maps, *Chaos Solitons and Fractals* **40**, 1697 (May 2009).